iScience

CellPress
OPEN ACCESS

Article

Restoring vision in adult amblyopia by enhancing plasticity through deletion of the transcriptional repressor REST

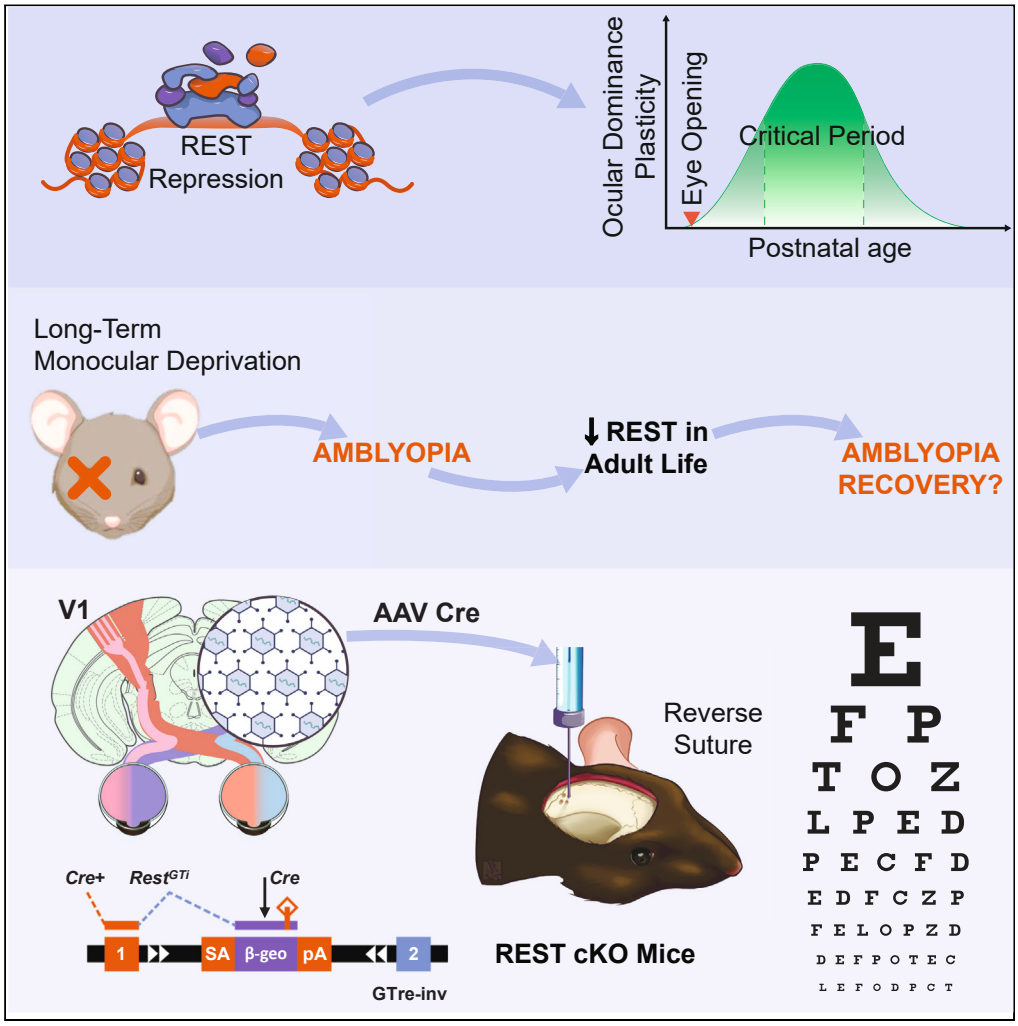

Dmytro Shmal, Giulia Mantero, Thomas Floss, Fabio Benfenati, José Fernando Maya-Vetencourt

fabio.benfenati@iit.it (F.B.)
maya.vetencourt@unipi.it (J.F.M.-V.)

Highlights

Knockdown of the transcriptional repressor REST restores V1 plasticity in adult life

The reinstatement of plasticity rescues normal vision in adult amblyopic animals

Plasticity is associated with an enhanced expression of REST target plasticity genes

Plasticity results from a reduction of perineuronal nets around parvalbumin interneurons

Shmal et al., iScience 27, 109507
April 19, 2024
https://doi.org/10.1016/j.isci.2024.109507

iScience

CellPress
OPEN ACCESS

Article

Restoring vision in adult amblyopia by enhancing plasticity through deletion of the transcriptional repressor REST

Dmytro Shmal,[1,2] Giulia Mantero,[1,3] Thomas Floss,[4] Fabio Benfenati,[1,2,6,7,*] and José Fernando Maya-Vetencourt[1,5,6,*]

SUMMARY

Visual cortical plasticity is high during early life, but gradually decreases with development. This is due to the Otx2-driven maturation of intracortical inhibition that parallels the condensation of extracellular matrix components into perineuronal nets mainly around parvalbumin-positive GABAergic neurons. Repressor Element 1 Silencing Transcription (REST) epigenetically controls the expression of a plethora of neuron-specific genes. We demonstrate that the conditional knockout of REST in the primary visual cortex of adult mice induces a shift of ocular dominance after short-term monocular deprivation and promotes the recovery of vision in long-term deprived animals after reverse suture. These phenomena paralleled a reduction of perineuronal net density and increased expression of REST target genes, but not of the homeoprotein Otx2 in the visual cortex contralateral to the deprived eye. This shows that REST regulates adult visual cortical plasticity and is a potential therapeutic target to restore vision in adult amblyopia by enhancing V1 plasticity.

INTRODUCTION

The extent to which the functional development of the brain relies on sensory inputs has been extensively studied in the primary visual system (V1). Neuronal circuitries in V1 markedly change as a function of experience during the critical period (CP) in early development, but this phase of heightened plasticity decreases over time.[1,2] Sensory experience modifies cortical networks via the activation of physiological processes that modulate gene transcription. V1 plasticity occurs through signal transduction pathways that promote epigenetic chromatin remodeling, which, in turn, modulates the activity of transcription factors.[3,4] This drives the expression of downstream target genes whose products operate changes in synaptic transmission and connectivity.[5,6]

Among the transcription factors that can be implicated in mediating the effects of sensory inputs on cortical plasticity, the Repressor Element 1 (RE1)-Silencing Transcription factor/Neural Restrictive Silencer Factor (REST/NRSF, henceforth referred to as REST) has recently attracted much interest. REST is mostly known as a master repressor of the transcription of a large cluster of genes, the majority of which are implicated in neural development and plasticity, such as growth factors, ion channels, synaptic vesicle proteins, neurotransmitter synthesizing enzymes, cytoskeletal proteins and others.[7] REST binds to gene promoters containing RE1 *consensus* sites and acts as a scaffold[8] to recruit the co-repressors mSin3[9] and CoREST[10] at its N- and C-terminal domains, respectively, as well as histone modifying enzymes. This complex modifies critical loci in DNA and histones, densely packing the genomic material and resulting in the transcriptional repression of RE1-containing genes.[11]

The expression of REST progressively decreases from embryogenesis to advanced stages of neural development due to a post-translational mechanism,[12] relieving repression from previously silenced neuron-specific genes that trigger neuronal differentiation.[13–15] It has been demonstrated that REST orchestrates complex homeostatic responses to long-term neuronal hyperactivity that restore physiological network activity by downscaling intrinsic excitability and synaptic transmission of excitatory neurons and potentiating the inhibitory control onto excitatory neurons.[16–18] Moreover, REST levels are upregulated *in vivo* by kainate-induced seizures[19–21] and progressively increase during aging in cortical neurons of healthy individuals with extended longevity.[22,23] Since cortical plasticity requires a tight control of network excitability that facilitates the reorganization of neuronal circuitries in response to experience, REST could be physiologically

[1]Center for Synaptic Neuroscience and Technology, Istituto Italiano di Tecnologia, Genova, Italy
[2]IRCCS Ospedale Policlinico San Martino, Genova, Italy
[3]Department of Experimental Medicine, University of Genova, Genova, Italy
[4]Helmholtz Zentrum München, Deutsches Forschungszentrum für Gesundheit und Umwelt, Neuherberg, Germany
[5]Department of Biology, University of Pisa, Pisa, Italy
[6]These authors contributed equally
[7]Lead contact
*Correspondence: fabio.benfenati@iit.it (F.B.), maya.vetencourt@unipi.it (J.F.M.-V.)
https://doi.org/10.1016/j.isci.2024.109507

implicated in driving homeostatic responses that control the establishment of experience-dependent cortical plasticity. In line with this notion, different homeostatic mechanisms assist to maintain neuronal activity within normal levels as modifications of neuronal circuitries take place in V1.[24]

As the visual cortex represents a well-established model of brain plasticity[3,25,26] and a developmental downregulation of histone post-translational modifications is known to modulate visual cortex plasticity,[27] we sought that REST could regulate V1 plasticity in the adult life after the end of the CP. We investigated the effect of REST downregulation on V1 plasticity in adult mice using two classical paradigms, namely the shift of ocular dominance (OD) after monocular deprivation (MD) and the recovery from vision degradation after sensory deprivation (amblyopia). These two plastic phenomena are restricted to early stages of development and are lost in adulthood because of a decline of V1 plasticity that occurs over time. This phenomenon has been largely attributed to Orthodenticle homeobox 2 (Otx2)-induced maturation of intracortical inhibition[28–30] and condensation of extracellular matrix components into perineuronal nets (PNNs) around parvalbumin (PV)-positive GABAergic neurons.[31–33] Here, we found that REST knockdown restores OD plasticity in adulthood. We also report that such degree of plasticity promotes the recovery from amblyopia late in life. Such phenomena were accompanied by an increased expression of REST downstream target genes and a concomitant reduction in the density of PNNs around fast-spiking PV-positive neurons in the binocular area (Oc1b) of V1 contralateral to the deprived eye, in the absence of changes in Otx2 levels.

RESULTS

Knockdown of REST in the primary visual cortex of adult conditional knockout mice

Adult REST^{GTi} mice were unilaterally microinjected into Oc1b with adeno-associated viruses (AAVs) expressing either Cre recombinase (Cre) or an inactive deletion mutant thereof (ΔCre) under the control of the CMV promoter and a GFP reporter (Figure 1A; Figure S1). Three weeks later, we verified the intensity and extension of the transduced cortical tissue by imaging GFP fluorescence (Figure 1B). GFP was expressed across all cortical layers (Figure 1C). RT-PCR of transduced cortical tissue showed that *Rest* mRNA was successfully reduced by Cre recombinase with respect to the ΔCre control (Figure 1D). Accordingly, the mRNA levels of representative neuron-specific REST target genes such as *Bdnf*, *Scn2a*, *Syn1* and *Npas4* revealed a concomitant and significant upregulation in the Cre-transduced cortex (Figure 1E). Conversely, non-RE1-containing plasticity genes preferentially expressed in pyramidal cells (*Arc*) or PV cells (*Fos, Egr4, Nr4a1*) displayed no significant changes in mRNA levels (Figures 1F and 1G). On the contrary, the astrocyte-specific Connexin-30 (*Cx30*), implicated in the closure of the CP for visual plasticity during development,[34] was significantly upregulated (Figure 1H), despite not being a canonical REST target.[35,36]

REST knockdown in adult mice impairs spatial resolution in the deprived eye after short-term monocular deprivation

We investigated whether a 3-day MD protocol in adult mice under conditions of REST knockdown in the Oc1b could lead to cortical plasticity responses associated with changes in spatial resolution. To this end, REST^{GTi} mice were transduced at postnatal day 90 (P90). After a 3-week interval (P110) to allow for recovery and Cre expression, recording multielectrode arrays were implanted in the Oc1b. After a 5-week recovery (P145), baseline behavioral and electrophysiological assessments were performed followed by short-term MD of the eye contralateral to the transduced V1. At P148, electrophysiology and behavior data were again gathered, and brains were transcardially perfused for immunofluorescent staining (Figure 2A). We first assessed the effects of MD on the optomotor response (OMR), which consists in compensatory head movements in response to the directional shifting of patterned visual stimuli. This gave us a behavioral readout of spatial resolution in V1, as the OMR relies on the perception of moving patterns on the vertical meridian with varying spatial frequencies. The overall OMR performance was quantified by calculating the areas under the OMR curves (AUC) collected at various spatial frequencies. While both naive, and Cre-transduced and ΔCre-transduced mice without MD showed comparable baseline acuity-driven behavior (Figure 2B), 3-day MD led to a significantly decreased OMR score at all tested spatial frequencies only in animals transduced with active Cre (Figure 2C), but not in naive or ΔCre-transduced mice, consistent with a decrease in spatial resolution typically observed after MD during early development. On the other hand, the OMR scores of ΔCre-transduced and naive mice after MD did not differ from the "*Before MD*" performance (compare Figure 2B with Figure 2C).

REST knockdown in adult mice allows a marked shift of ocular dominance in Oc1B in response to short-term monocular deprivation

In addition to the OMR, we also alternately recorded monocular visually evoked potentials (VEPs) before and after 3 days of MD using a chronic 16-channel microwire recording array implanted into the left V1 that had previously been transduced with either Cre- or ΔCre AAVs. Animals were connected to the recording setup by means of a tether cable and allowed to roam the enclosure freely, with visual flash stimuli provided by an overhead white LED. The comparison of the averaged visually evoked potential (VEP) amplitudes obtained from separately stimulating the right and the left eyes allows to calculate the contra-to-ipsi (C/I) ratio, a measure of OD. Physiologically, this value is between 2 and 3, reflecting contralateral eye dominance in Oc1b. During the juvenile CP for V1 plasticity, 3 days of MD shift OD toward the open eye, whereas in adults the C/I ratio is insensitive to MD. While in our adult naive and ΔCre-transduced controls, the 3-day MD was unable to modify the C/I ratio, REST knocked down mice experienced a significant change in OD toward the non-deprived ipsilateral eye (Figure 3), consistent with a reactivation of cortical plasticity.[37] It is known that OD plasticity in juvenile mice is dominated by a drop of the closed eye response strength, whereas adult mice OD shifts are primarily due to an increase in the open eye strength.[38,39] To examine

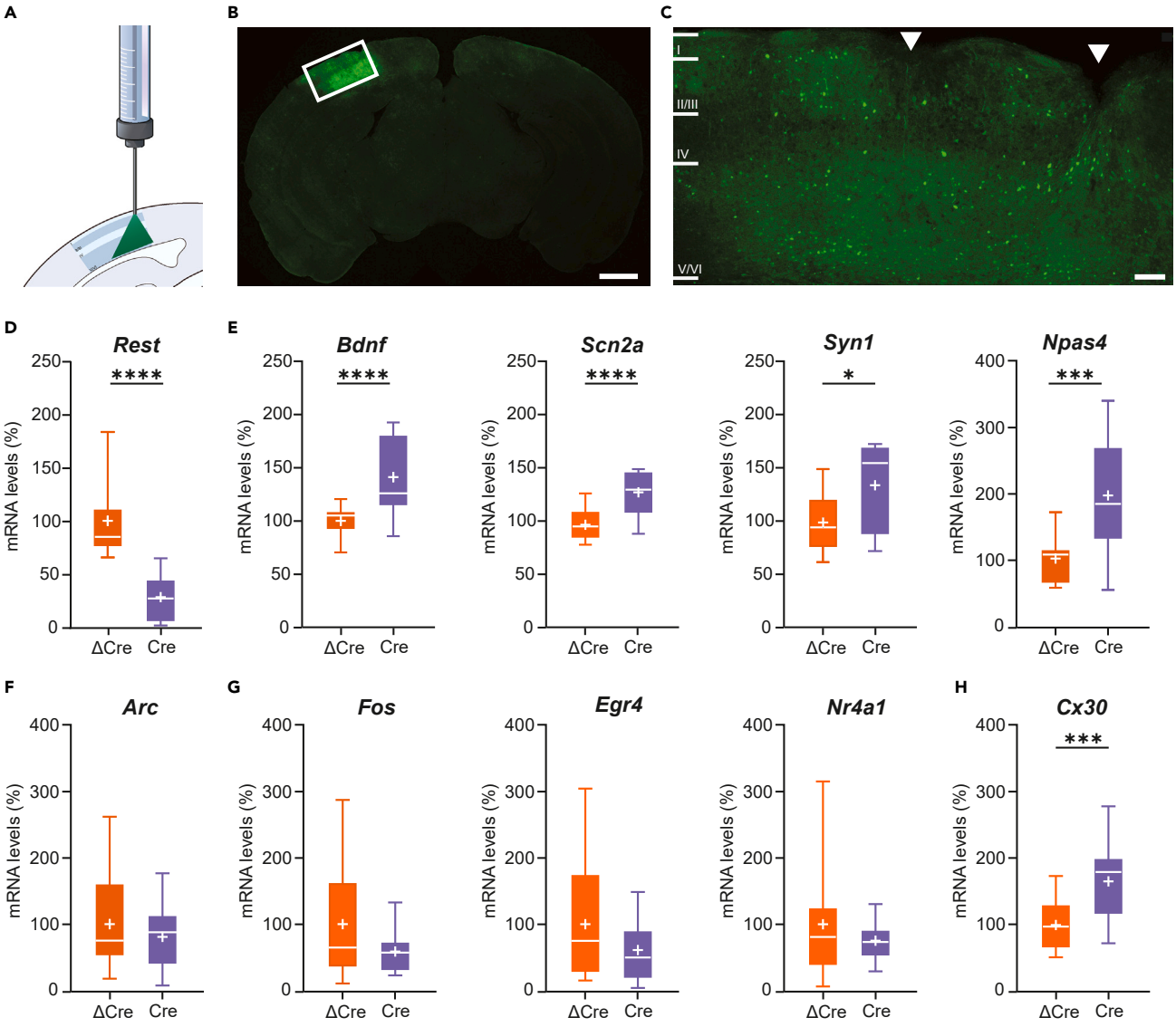

Figure 1. Cre-dependent knockdown of REST in the Oc1b in REST^{GTi} mice

(A) Schematic illustration of stereotaxic delivery of AAV9 carrying either Cre or ΔCre into the Oc1b of adult REST^{GTi} mice.

(B) Representative confocal image of a coronal brain slice at the level of V1, showing GFP expression in the hemisphere transduced with Cre-expressing AAV9 (green). Scale bar, 1 mm.

(C) Higher magnification of Oc1b indicated by the rectangle in panel b. Arrowheads indicate the injection sites. Scale bar, 100 μm.

(D) Boxplot of the *Rest* mRNA levels. Animals transduced with active Cre showed a marked reduction of *Rest* mRNA levels in V1 compared to the ΔCre-transduced group.

(E) Boxplots of the mRNA levels of REST target genes. Animals transduced with active Cre showed increased mRNA levels of known plasticity genes such as *Bdnf*, *Scn2a*, *Syn1*, and *Npas4*.

(F–H) Boxplots of the mRNA levels of plasticity genes that are not REST targets. No significant changes were observed in genes preferentially expressed by pyramidal neurons, such as *Arc* (F), and PV neurons, such as *Fos*, *Egr4*, and *Nr4a1* (G), while the mRNA levels of the *Cx30* gene preferentially expressed in astrocytes were increased (H). In panels D–H, data were normalized to the mean of the ΔCre-transduced group. *p < 0.05, ***p < 0.001, ****p < 0.0001; Mann-Whitney *U*-test; (n = 16 for both ΔCre and Cre groups). For exact p values and source data, see Data S1. See also Figure S1 and Table S1.

which of the two components contributes to the restoration of OD plasticity in V1 caused by REST downregulation, we compared VEP amplitudes after stimulation of either eye in Cre and ΔCre transduced mice. A significant reduction of the response to stimulation of the deprived eye 3 days after MD was evident in Cre-treated animals while no difference in the open eye strength was observed after ΔCre transduction (Figure S2). This indicates that the V1 plasticity induced by REST downregulation mimics that observed during early stages of brain development.

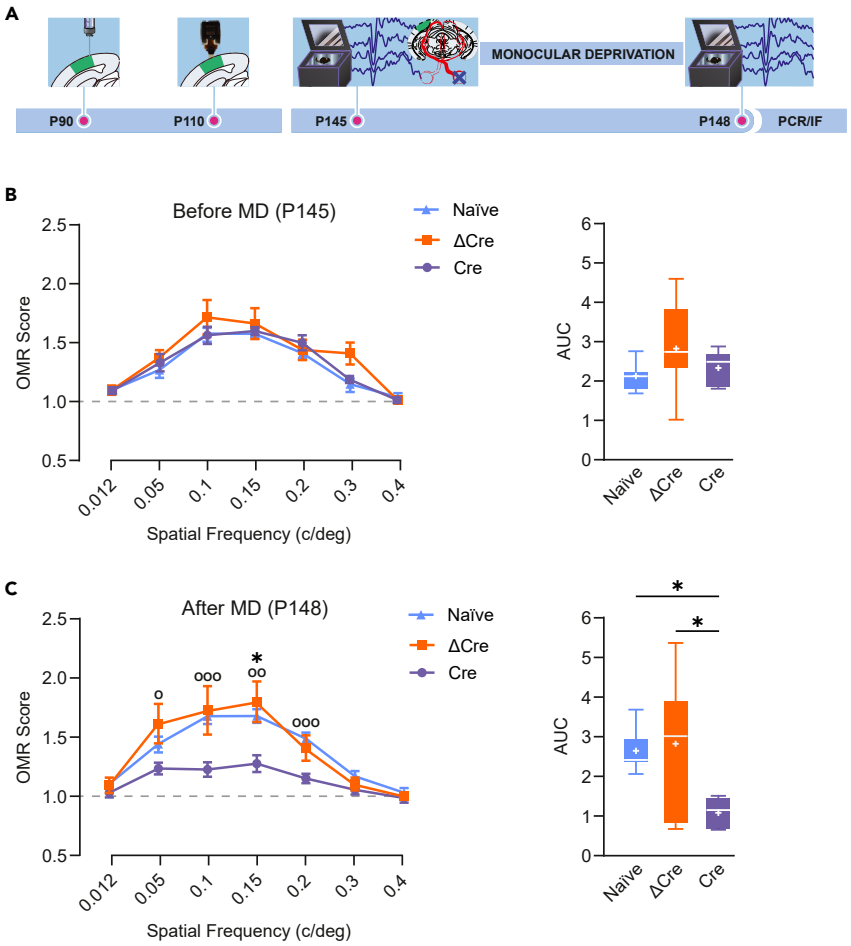

Figure 2. Impaired spatial resolution in the deprived eye after 3-day MD in adult REST cKO mice

(A) Experimental timeline.

(B and C) OMR responses of naive, Cre-transduced and ΔCre-transduced mice before (B) and after (C) 3 days MD. *Left:* OMR performance curves. Data are means ± s.e.m. *$p < 0.05$, Cre vs. ΔCre; $^{○}p < 0.05$, $^{○○}p < 0.01$, $^{○○○}p < 0.001$, Cre vs. naive; repeated measures two-way ANOVA/Holm-Sidak tests. *Right:* Boxplots of the overall OMR performance quantified by calculating the area under the OMR curves (AUC). *$p < 0.05$; one-way ANOVA/Tukey's test. Before deprivation, the three experimental groups show similar OMRs at all spatial frequencies, while, after 3-day MD, only Cre-transduced animals displayed a markedly reduced OMR score at all spatial frequencies (n = 11, 7 and 5 for naive, ΔCre and Cre groups, respectively). For exact p values and source data, see Data S1.

Ocular dominance and OMR changes after short-term monocular deprivation in the adult correlate with REST knockdown and upregulation of its target genes

To confirm the dependence of the OD shift and reduced spatial resolution on REST cKO, we examined the intraindividual correlations between *REST* mRNA levels, expression of its target genes, OMR scores and VEP C/I ratios. Firstly, we constructed a covariance matrix of these variables including only animals that successfully underwent all experimental procedures from the Cre- and ΔCre-transduced groups. We observed that the extent of REST knockdown positively correlated with the shift in OD evidenced by the variation of the C/I ratio (Δ C/I) and reduction in spatial resolution-driven behavior at 0.1 and 0.15 c/deg (Δ OMR 0.1 and Δ OMR 0.15) after 3-day MD. This was paralleled by a strong inverse correlation with the upregulated REST target gene mRNAs *Bdnf, Scn2a, Syn1* and *Npas4* (Figure 4A). Building on this covariance matrix, we centered the dataset and performed principal component analysis (PCA). Plotting the scores from the first 3 principal components, we observed that Cre-transduced animals tend to displace a similar, longer distance along the same orientation and approximate direction in principle component space between the two states, while ΔCre-transduced animals seem to displace indifferently with no preference for distance, direction or orientation. To quantify this phenomenon, we plotted the displacement of each animal along the principal component 1 (PC1), which accounted for the majority of total variance in the dataset (57%). While the mean displacement of the ΔCre group was close to 0, the Cre-transduced animals clustered closely around a significantly higher positive value (Figure 4B).

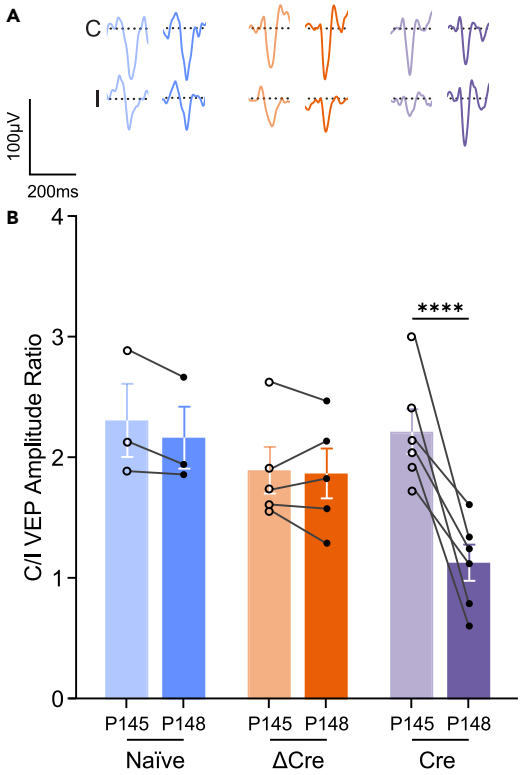

Figure 3. Marked shift of OD in Oc1b after 3-day MD in adult REST cKO mice

(A) Representative VEP traces from monocular recordings before and after 3-day MD in naive, ΔCre-transduced and Cre-transduced REST^{GTi} mice in response to 200 ms white LED flash stimulation.

(B) VEP-derived C/I ratios before and after 3 days of MD in the three experimental groups. Cre-transduced animals demonstrate a marked OD shift following 3 days of MD, while the OD of naive and ΔCre-transduced is unaffected. Bar plots show means ± s.e.m. with superimposed individual experimental data. ****$p < 0.01$; repeated measures two-way ANOVA/Holm-Sidak tests (n = 3, 5 and 6 for naive, ΔCre and Cre groups, respectively). For exact p values and source data, see Data S1. See also Figure S2.

Short-term monocular deprivation plasticity in adult REST cKO mice is associated with a lower number of parvalbumin-positive cells ensheathed in perineuronal nets

A key factor in the regulation of the time course of CP plasticity in V1 is the development of PV-positive inhibitory interneurons, and the formation of condensed extracellular matrix into PNNs around them. PNNs enable the internalization of the homeoprotein Otx2 by PV neurons, driving their activity-dependent maturation.[30,40] To verify an involvement of PV interneurons and PNNs in the observed effects, we bilaterally immunostained Oc1b-containing cortical slices from naive, ΔCre- and Cre-transduced REST^{GTi} mice with *Wisteria floribunda* lectin (WFA) for PNNs and antibodies targeting PV and Otx2. Cell counts, comprising all cortical layers and filtered for profiles >15 μm (Figure S3), show a significant reduction of cells double-positive for PNNs and PV in the Oc1b of Cre-transduced mice, while the number of PV/PNN-positive neurons was virtually unaffected in naive and ΔCre-transduced controls (Figures 5A–5C). These data suggest the presence of a lowered inhibitory tone in Oc1b associated with REST knockdown. No differences were observed in the mean Otx2 fluorescence in PV cells across the three experimental groups (Figures 5A–5D).

PV neurons have been described to be infected by AAV9 and transduced by the ubiquitous CMV promoter.[41] Nevertheless, we wanted to evaluate, under our experimental conditions, whether PV neurons were effectively transduced and whether the changes observed in the number of PV-positive and PV/PNN-positive neurons were specific for the GFP-expressing PV neurons transduced with Cre. Thus, we computed the total number of PV-positive and PV/PNN-positive cells and compared it with that of GFP/PV/PNN-positive cells alternately transduced with either Cre or ΔCre. The data show that the observed changes are only present in the subpopulation of PV-positive and PV/PNN-positive cells that had been transduced with Cre, and not with the control ΔCre, indicating that the effects are cell-autonomous, and directly attributable to the REST deletion (Figure S4).

REST knockdown improves spatial resolution in adult amblyopic animals

Next, we evaluated whether the plastic effects of REST knockdown could promote the recovery from experimentally induced amblyopia. This condition was induced in REST^{GTi} mice by eyelid suture of the right eye soon after opening at P21, maintaining it in place until P110. At P75,

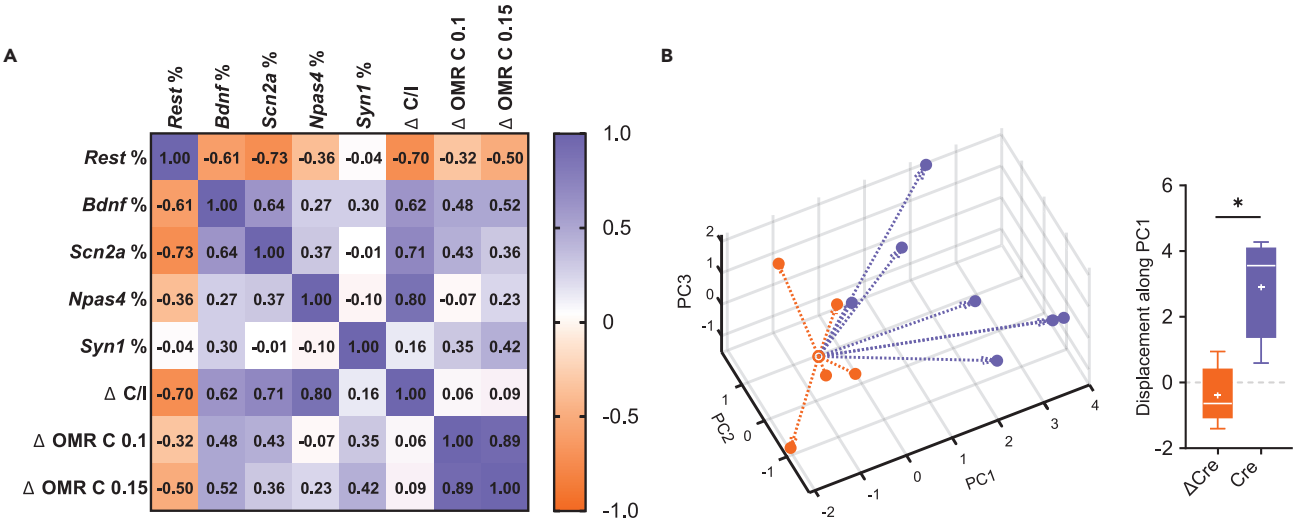

Figure 4. The variations in C/I ratio and OMR score after 3-day MD show correlation and covariance with knockdown of *Rest* and upregulation of its target genes

(A) Pearson's correlation grid of mRNA expression levels of *Rest*, its target genes *Bdnf*, *Scn2a*, *Npas4*, and *Syn1*, the variation of C/I ratio before and after 3 days of MD (Δ C/I) and the variation in OMR score before and after MD at 0.1 (Δ OMR 0.1) and 0.15 c/deg (Δ OMR 0.15). The values of the correlation coefficient "r" are indicated in the pseudo-color scale on the right. REST expression shows strong inverse correlation with the changes in OD and acuity-driven behavior.

(B) *Left:* Principal component analysis. 3D line plots show the trajectories of each animal in the principal component space during MD, to visualize covariance. The empty circle represents the "before MD" state, the filled circles refer to the "after MD" state and dotted arrows mark the trajectories. The variables loaded into the PCA are the same used in the correlation grid. Cre-transduced animals show clear co-directionality and covariance, while the ΔCre group does not. *Right:* The boxplot shows the before-after displacement distance along the principal component 1 (PC1), which accounts for the majority of variance in the system. *$p < 0.05$; Mann-Whitney's *U*-test (n = 5 for both ΔCre and Cre). For exact p values and source data, see Data S1.

AAVs expressing either Cre or ΔCre were injected into the left Oc1b. At P95, recording arrays were implanted. At P110, baseline behavioral and electrophysiological recordings were performed, and the reverse suture (RS) was applied. Fifteen days later (P125), electrophysiology and behavior were recorded again. Brains were then transcardially perfused for immunofluorescence as described above (Figure 6A). In the amblyopia model, OMR was analyzed using an eye separation algorithm to extrapolate the role of each eye in the physiological responses. Before RS, the long-term deprived right eye ("*Contra*" to the transduced left V1) in naive, Cre-transduced, and ΔCre-transduced mice showed no measurable contribution to spatial resolution-dependent behavior (Figure 6B), in contrast to the stable contribution of the non-deprived "*Ipsi*" eye (Figure 6D) and consistent with the amblyopia phenotype. Interestingly, 15 days of RS in the Cre-transduced mice, but not in naive or ΔCre-transduced mice, led to a significant recovery of the "*Contra*" eye at the OMR score for spatial resolutions of 0.15 and 0.20 c/deg (Figure 6C), while no improvement was observed in ΔCre-transduced controls. Note the absence of significant changes in the "*Ipsi*" component of naive, Cre- and ΔCre-transduced groups at both P110 and P125 time points (Figures 6D and 6E).

REST knockdown in adult mice rescues binocularity in adult amblyopic animals

To assess whether REST knockdown can rescue binocularity in adult amblyopic mice after 15 days of RS, we performed alternate VEP recordings before and after the inverse deprivation. Firstly, the long-term deprived eye contralateral to the transduced V1 was opened and the responses from each eye were recorded separately ("*Before*"). Successively, the ipsilateral eye to the transduced V1 was left deprived for 15 days, after which recordings for both eyes were performed again ("*After*"). Long-term MD reduced C/I ratios in all animals to approximately 1. Notably, Cre-transduced animals demonstrated a significant recovery of OD after 15 days of RS to a level comparable to untreated controls, whereas no C/I ratio recovery was observed in naive and ΔCre-transduced controls (Figure 7). The rescue of binocularity in adult amblyopic mice was due to a statistically significant increase of the deprived eye strength (Figure S5).

The recovery of ocular dominance in amblyopic mice correlates with REST knockdown and upregulation of its target genes

The covariance matrix of the Cre- and ΔCre-transduced groups highlights the robust inverse co-linearity of *Rest* knockdown with recovery of OD (Δ C/I ratio) and OMR scores at 0.15 and 0.20 c/deg (Δ OMR 0.1 and Δ OMR 0.15) after RS, as well as with the increase in the REST target genes *Bdnf*, *Scn2a, Syn1* and *Npas4* (Figure 8A). Subsequently, we collated all data before and after the reverse suture (from P110 to P125) and ran a PCA, wherein PC space trajectories of Cre-transduced animals immediately exhibited a striking parallelism and direction preference, moving away from the cluster of P110 starting points. ΔCre-transduced animals on the other hand, did not meaningfully depart from this P110 cluster (Figure 8B, *left*). For this dataset, PC1 explained an even greater share of total variance (92%), and the mean displacement along PC1 was highly significant for Cre-transduce cKO mice, while for the ΔCre-transduced group was again close to 0 (Figure 8B, *right*).

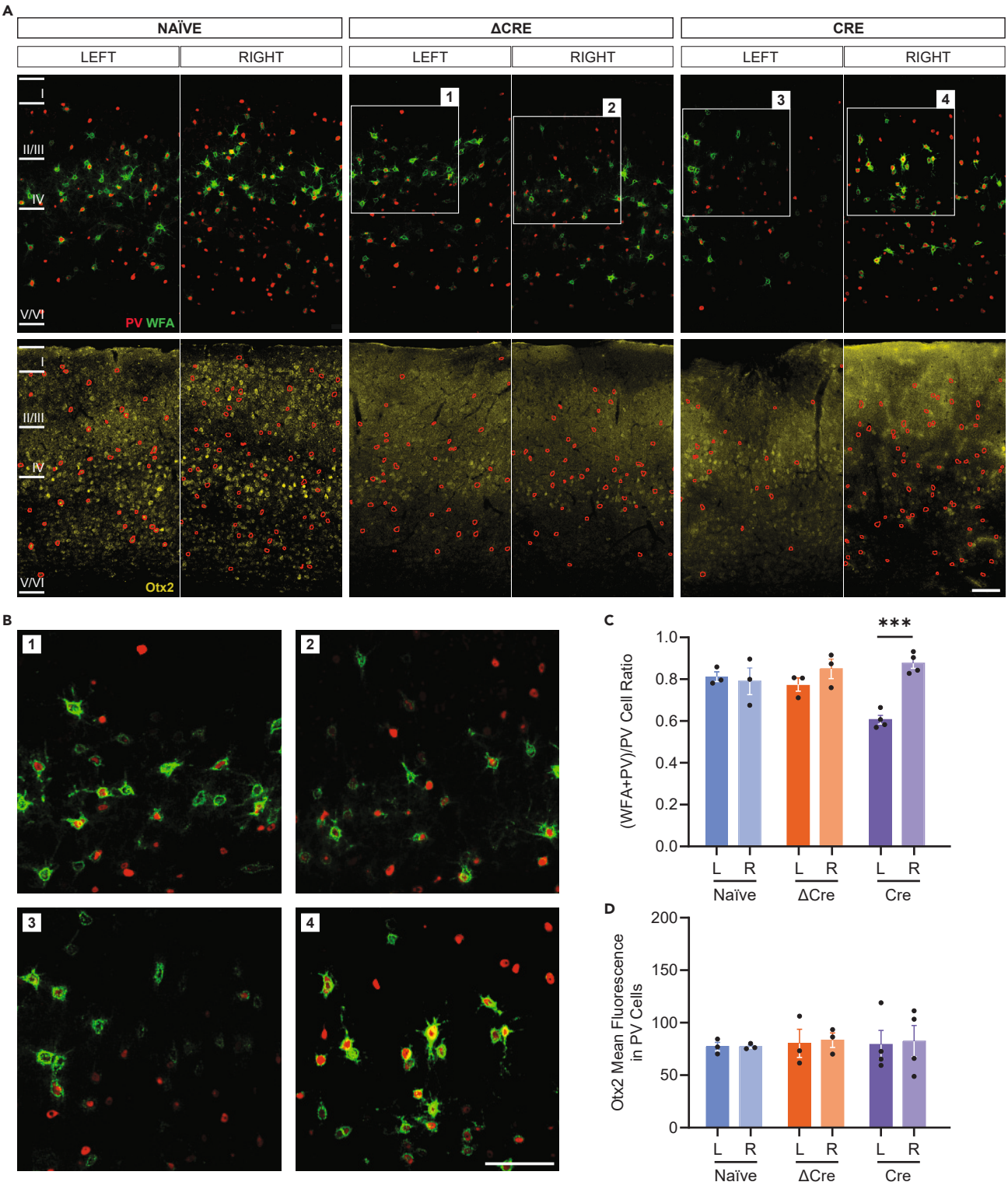

Figure 5. Parvalbumin-positive cells ensheathed in PNNs are decreased after 3-day MD in adult REST cKO mice

(A) Representative confocal images of left and right Oc1b from naive (left column), ΔCre-transduced (middle column) and Cre-transduced (right column) REST^{GTi} mice immunolabelled with anti-parvalbumin antibodies and WFA (green respectively; first row) and anti-Otx2 antibodies (yellow, second row). Outlines of PV cells are superimposed onto Otx2 images (red circles) to indicate the regions-of-interest (ROIs) that have been analyzed. The PV channel has been denoised to clearly depict cell somata.

Figure 5. *Continued*

(B) High magnification of layers II, III and IV from the corresponding images in panel a: ΔCre-transduced left Oc1b (1); ΔCre-transduced right Oc1b (2); Cre-transduced left Oc1b (3); Cre-transduced right Oc1b (4). Scale bars, 100 μm.

(C) Bar plot showing the ratio of the number of PNN-ensheathed PV neurons to total PV neurons with superimposed individual experimental points. The Cre-transduced cortical area contralateral to the deprived eye shows a stark decrease in PV/PNN-positive cells with respect to the untreated contralateral hemisphere.

(D) No changes were observed in the Otx2 mean fluorescence of PV neurons. Bar plots show means ± s.e.m. with superimposed individual experimental data. ***$p < 0.001$; one-way ANOVA/Dunnett's tests (n = 3, 3 and 4 for naive, ΔCre- and Cre-transduced mice, respectively). For exact p values and source data, see Data S1. See also Figures S3 and S4.

The recovery of ocular dominance and spatial resolution in amblyopic REST cKO mice is associated with fewer parvalbumin-positive cells surrounded by PNNs in Oc1b

We finally investigated whether PV interneurons and their PNNs in V1 were affected by long-term MD and their changes could contribute to the recovery of OD in this model of amblyopia. To this aim, we bilaterally immunostained Oc1b-containing cortical slices from naive, ΔCre- and Cre-transduced $REST^{GTi}$ mice with WFA for visualizing PNNs, anti-PV and anti-Otx2 antibodies. Similar to what we observed for the short-term MD paradigm, counts across all layers showed a strong reduction in PNN-positive PV cells only in the Oc1b of Cre-transduced mice (Figures 9A–9C), while no differences were detected in the mean Otx2 fluorescence in PV interneurons across the three experimental groups (Figures 9A–9D). Also in this experimental paradigm, we evaluated the counts of non-transduced, Cre-transduced and ΔCre-transduced PV-positive and PV/PNN-positive cells (Figure S6). The data show again that the observed changes are only present in the subpopulation of PV and PV/PNN-positive cells that had been transduced with Cre, demonstrating that they are causally induced by REST deletion. Taken together, the data suggest a role for decreased cortical inhibitory tone in the recovery of cortical plasticity both after short-term MD and in this model of amblyopia.

DISCUSSION

The process of plasticity reactivation in adult V1 is a hot spot in current neuroscience research. It is a multifactorial event that includes distinct cellular and molecular mechanisms that, through the activation of intracellular signal transduction pathways, regulate the expression of genes that modify synaptic transmission.[4,27,33,42–54] The results of the present study unveil a previously unknown role for the transcriptional repressor REST, a master regulator of neuron-specific genes, in mediating the reinstatement of plasticity in the adult V1. We show that 3 days of MD cause a significant shift of OD and impaired spatial resolution in adult animals in which REST has been knocked down. Because these plastic phenomena are restricted to early stages of development, our findings indicate that a reduction of REST expression in adulthood reactivates V1 plasticity. Remarkably, the enhancement of plasticity induced by REST downregulation in V1 also promotes the recovery of binocularity and acuity-driven behavior in adult amblyopia.

As the knockdown of REST was performed at an age (>P125) that goes beyond the temporal window (P110) in which there is still some degree of plasticity in V1,[55] our findings suggest that, under physiological conditions, REST takes part in the mechanisms that prevent V1 plasticity in adulthood probably by exerting an inhibitory constraint on the expression of plasticity genes. Such an assertion is supported by the fact that the knockdown of REST in V1 is associated with an enhanced expression of downstream target genes such as *Bdnf, Npas4, Scn2a, Syn1*[7] that are involved in V1 structural and functional plasticity. This demonstrates that local REST downregulation turns on a transcriptional program that provides a permissive environment for plasticity and facilitates the functional reorganization of neuronal circuitries during this phase of enhanced plasticity. Notwithstanding the use of a CMV promoter used to express Cre and knockout REST in V1, the upregulation of neuron-specific genes in the Cre-transduced V1 testifies that neurons are directly involved in the physiological responses to MD.

We found that the degree of plasticity induced by REST knockdown in V1 was associated with a marked decrease in PV/PNN+ neurons in both adult short-term MD animals and adult amblyopic mice after RS. These data are consistent with the observation that pharmacological blockade of intracortical inhibitory transmission is able to reinstate V1 plasticity after the end of the CP.[48] Our findings suggest a potential role for a decreased inhibitory tone in the recovery of cortical plasticity induced by REST downregulation. It has been demonstrated that the Otx2-induced maturation of intracortical inhibition causes the end of plasticity in V1[28–30] and that disruption of Otx2 localization to PV cells reduces PNN density and reopens plasticity in adult mice.[32,40] Interestingly, under our experimental conditions, the decrease in PV/PNN+ neurons due to REST deletion occurred in the absence of any change in Otx2 levels in V1.

Our results support a model in which REST deletion promotes a deficit in the number of PV/PNN+ cells in V1 which, in turn, decreases the inhibitory tone and sets in motion the process of plasticity reactivation in adulthood. The reduction in PV/PNN+ neurons is likely a cell autonomous effect of REST deletion, as the decrease in PV cell number and PNNs only occurs in the population of GFP+ PV neurons that had been transduced with Cre recombinase. A similar decrease of PNNs in V1, associated with increase of OD plasticity, has been obtained in adult mice by inhibition of the microRNA miR29a, which regulates expression of the extracellular matrix.[53]

Given the ubiquitous CMV promoter used, it is possible that deletion of REST in pyramidal neurons and/or astrocytes could also contribute to the PNN decrease. We have previously shown that REST KO primary astrocytes increase neuronal excitability by decreasing K^+ buffering and synaptic glutamate uptake.[56] In this context, the observed transcriptional increase of astrocyte Connexin-30, which during development contributes to the closure of the plasticity window, could represent a homeostatic mechanism during a phase of enhanced plasticity in adult

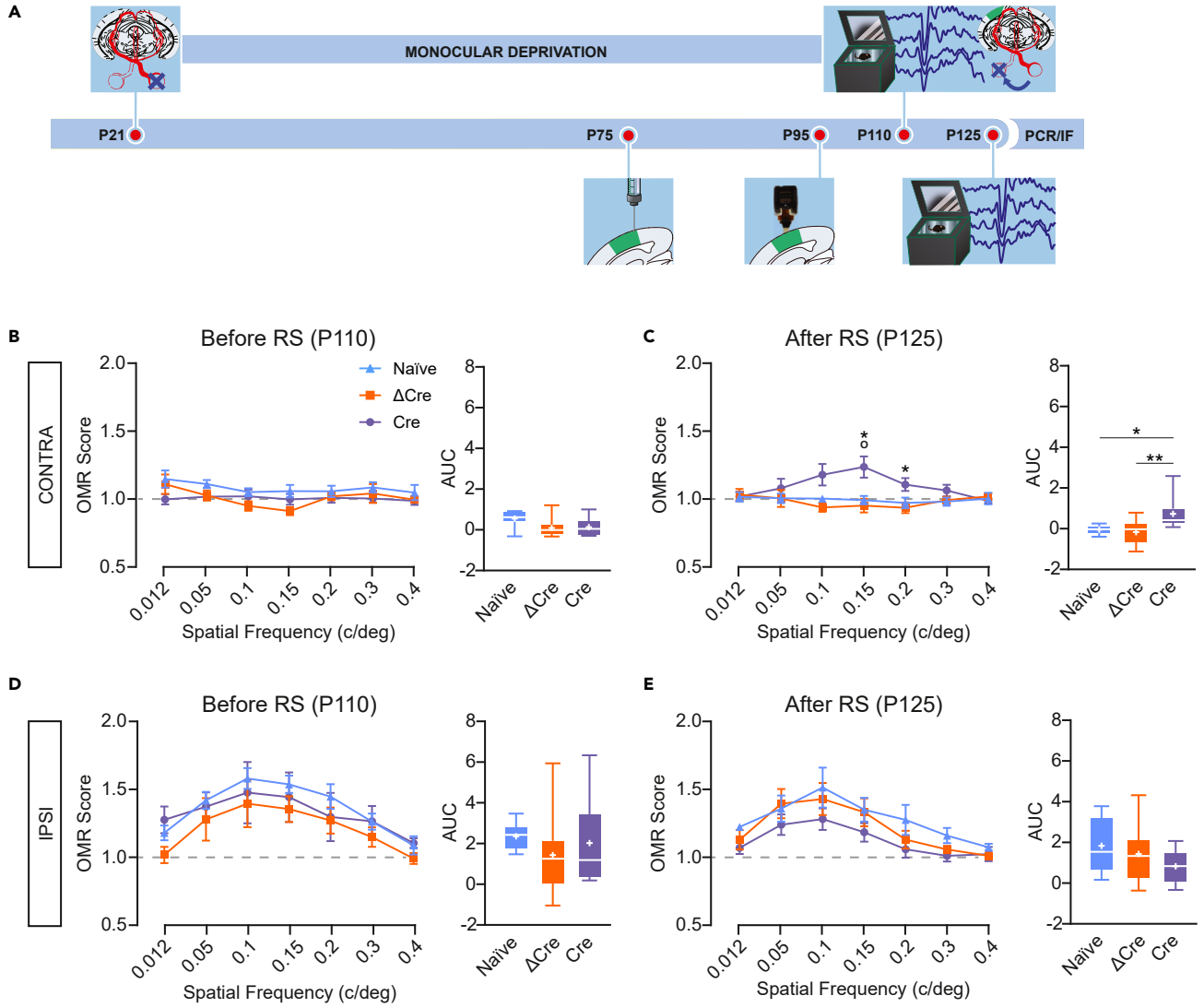

Figure 6. REST knockdown enables recovery of amblyopia-associated loss of spatial resolution after 15 days of reverse suture

(A) Timeline of experiments.

(B and C) Software-separated OMR performance traces for the contralateral long-term deprived eye (Right eye, "*Contra*") before (P110) and after (P125) 15-day reverse suture. At P125, Cre-transduced, but not naive or ΔCre-transduced, animals showed partial recovery of spatial resolution-driven behavior at 0.15 and 0.2 c/deg, paralleled by an increased AUC (see boxplots on the right).

(D and E) No significant changes were observed concerning the ipsilateral (Left eye, "*Ipsi*") eye component. Data in the OMR performance traces are means ± s.e.m.; *p < 0.05, Cre vs. ΔCre; °p < 0.05, Cre vs. naive; repeated measures two-way ANOVA/Holm-Sidak's tests. For boxplots *p < 0.05, **p < 0.01; one-way ANOVA/Tukey's test (n = 8, 10 and 8 mice for naive, ΔCre and Cre, respectively). For exact p values and source data, see Data S1.

life. It will be interesting to evaluate whether the plasticizing effects of REST downregulation occur, at least in part, through these mechanisms or whether there are different pathways leading to the reinstatement of V1 plasticity.

Another interesting result is the upregulation of *Bdnf* and *Npas4* upon REST downregulation, as these two genes have been previously associated to the regulation of V1 plasticity in the adult life. Indeed, intracortical infusion of BDNF[54] or activation of TrkB[57] reinstates susceptibility to sensory deprivation in adulthood. Moreover, it has been reported that a decreased density of PNNs onto PV interneurons increases the phosphorylation state of TrkB through the dissociation of the receptor protein tyrosine phosphatase σ from PNN components.[58,59] Combined with the higher expression of BDNF due to REST inactivation, this could translate into an increased TrkB signaling in PV neurons that decreases the expression of PV and Kv3 channels, resulting in the loss of their characteristic fast-spiking behavior.[57]

It has been reported that overexpression of the transcription factor Npas4 is necessary and sufficient to restore adult V1 plasticity.[45] Consistently, Npas4 has been previously reported to affect excitatory transmission and promote the development of inhibitory synapses that control the balance between synaptic excitation and inhibition in cultured neurons.[60,61] Being a REST downstream target, an increased expression of

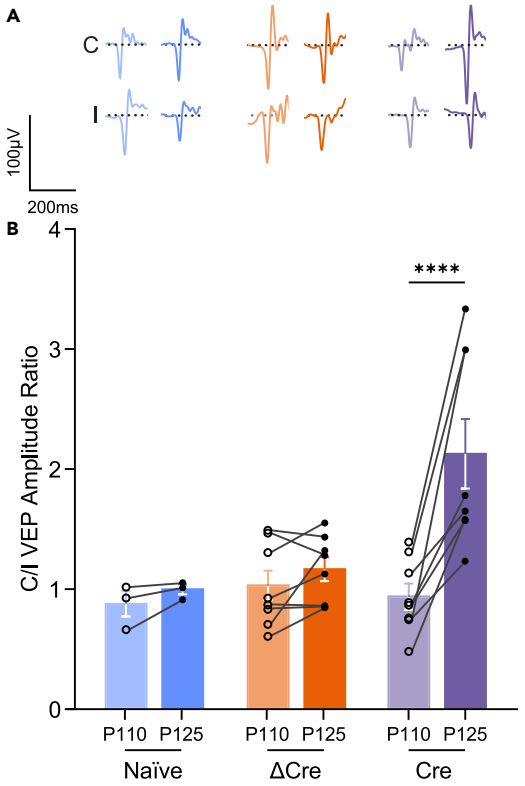

Figure 7. REST knockout rescues binocularity in adult amblyopic animals after 15-day RS

(A) Representative VEP traces from monocular recordings before and after 15-day reverse suture in naive (orange), ΔCre-transduced (blue) and Cre-transduced (green) $REST^{GTi}$ mice in response to 200 ms white LED flash stimulation.

(B) VEP-derived C/I ratios before and after RS in the three experimental groups. Cre-transduced mice experienced a significant recovery of OD following RS, while naive and ΔCre-transduced did not. Bar plots show means ± s.e.m. with superimposed individual experimental data. ****$p < 0.01$; repeated measures two-way ANOVA/Holm-Sidak tests (n = 3, 8 and 8 for naive, ΔCre and Cre groups, respectively). For exact p values and source data, see Data S1. See also Figure S5.

Npas4 could mediate some of the responses driven by REST downregulation needed for the process of plasticity reactivation in V1.[24] Furthermore, Npas4 has also been involved in the occurrence of plastic phenomena in other brain regions. In the CA3 area of the hippocampus, for instance, Npas4 regulates a transcriptional program that is required for contextual memory formation,[62] while in the DG it drives a transcriptional pathway crucial for contextual fear memory engrams.[63]

The capacity of the brain to change structurally and functionally in response to experience is mostly active during early stages of development and decreases later in life when major alterations of neuronal networks no longer take place in response to experience. In experimental animals, various pharmacological,[40,50,54,64,65] environmental,[43,66] and genetic[49] approaches reported the rescue of visual acuity in the adult life. In humans, the recovery of acuity after long-term sensory deprivation has been reported in adult anisometropic amblyopes after physical exercise combined with inverse occlusion.[67] Likewise, perceptual learning seems to be an effective strategy to improve vision in adult amblyopia.[68–70] More recently, a significant improvement of vision in adult anisometropic and/or strabismic patients has been reported after a 12-week treatment with the acetylcholinesterase inhibitor donepezil.[71]

The possibility to non-invasively enhance plasticity in the adult brain represents an unmet need to treat a variety of pathological conditions in which a reorganization of neuronal networks could be beneficial. Our data identify the transcription factor REST as a new player into the context of cortical plasticity reactivation in the adult life. REST-mediated transcriptional mechanisms can be important therapeutic targets for future drug development. Modulating REST expression in the visual cortex using oligonucleotides or mRNA-silencing strategies may open a new potential avenue in the treatment of amblyopia by enhancing cortical plasticity.

Limitations of the study

Since a decrease in PNN may also decrease Otx2 uptake, the absence of changes in Otx2 immunoreactivity, although interesting, should be taken with caution. In fact, we cannot exclude that a small, but physiologically significant, change in Otx2 could be below the detection limit of our experimental approach, masked by the experimental variability, or have a slower timing than the decrease in PNNs.

Moreover, our use of a ubiquitous CMV promoter does not allow for discrimination of the involvement of different cell types in the observed effects, which warrants further studies utilizing cell type-specific viral promoters.

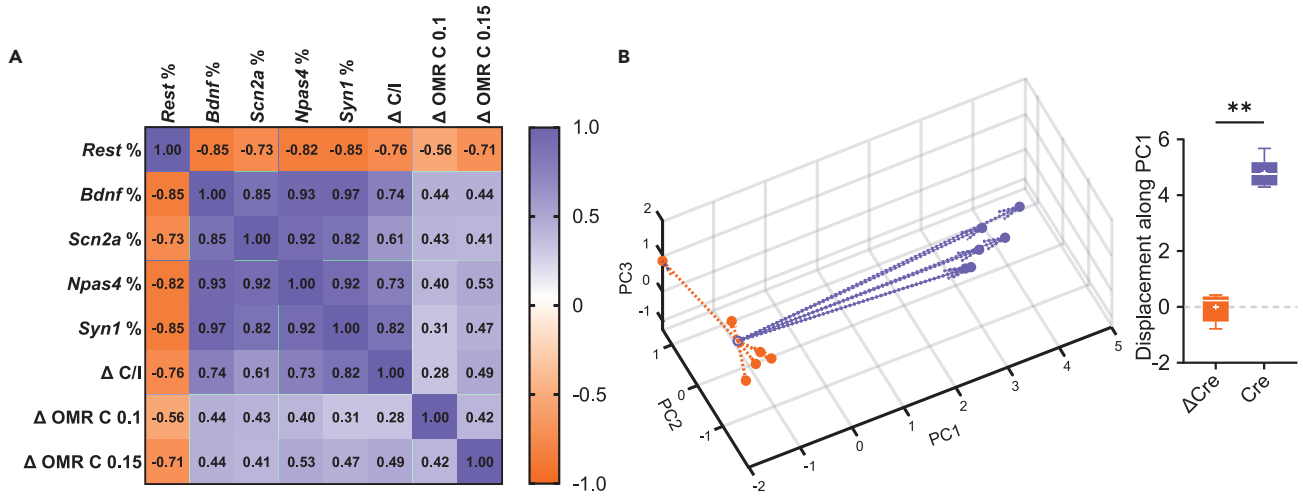

Figure 8. The recovery of OD and spatial resolution in amblyopic mice sharply correlates with the knockdown of REST and upregulation of its target genes

(A) Pearson's correlation grid of mRNA expression levels of *REST*, its target genes *Bdnf*, *Scn2a*, *Npas4*, and *Syn1*, the variation of C/I ratio from P110 to P125 (Δ C/I), and the variation in OMR score from P110 to P125 at 0.1 and 0.15 c/deg (Δ OMR 0.1 and Δ OMR 0.15, respectively). The values of the correlation coefficient "r" are indicated in the pseudo-color scale on the right. REST expression shows high inverse correlation with its target genes and the recovery in OD and acuity-driven behavior.

(B) *Left:* Principal component analysis. 3D line plots show the trajectories of each animal in the principal component space from P110 to P125. Empty circle represents the "*before RS*" state and filled circles are the "*after RS*" state, while dotted arrows mark the trajectory. The variables loaded into the PCA are the same used in the correlation grid. Cre-transduced animals (green) show definite co-directionality and covariance, while the ΔCre-transduced group (blue) does not. The boxplot shows the P110-P125 displacement distance along principal component 1 (PC1), which explains the majority of variance in the data. **p < 0.01; Mann-Whitney's *U*-test. (n = 6 for both ΔCre and Cre). For exact p values and source data, see Data S1.

STAR★METHODS

Detailed methods are provided in the online version of this paper and include the following:

- KEY RESOURCES TABLE
- RESOURCE AVAILABILITY
  - Lead contact
  - Materials availability
  - Data and code availability
- EXPERIMENTAL MODEL AND STUDY PARTICIPANT DETAILS
  - Murine model
- METHOD DETAILS
  - Intracortical microinjection for AAV-mediated transduction
  - Chronic microwire array implants
  - *In vivo* electrophysiology
  - Optomotor response
  - Real-time qPCR
  - Immunohistochemistry and morphometric analysis
- QUANTIFICATION AND STATISTICAL ANALYSIS

SUPPLEMENTAL INFORMATION

Supplemental information can be found online at https://doi.org/10.1016/j.isci.2024.109507.

ACKNOWLEDGMENTS

We are grateful to dr. Gail Mandel (Vollum Institute, Portland, OR) and the German Gene Trap Consortium (GGTC-Partners) for providing us with the REST conditional knockout mice; drs. Francesca Vacca, Laura Gennaccaro, Diego Moruzzo and Simona Francia for assistance in RT-PCR and immunohistochemistry experiments, and dr. Valentina Castagnola for help with the graphical abstract. We also thank drs. Riccardo Navone (Istituto Italiano di Tecnologia, Genova, Italy), Laura Emionite and Michele Cilli (IRCCS Ospedale Policlinico San Martino, Genova,

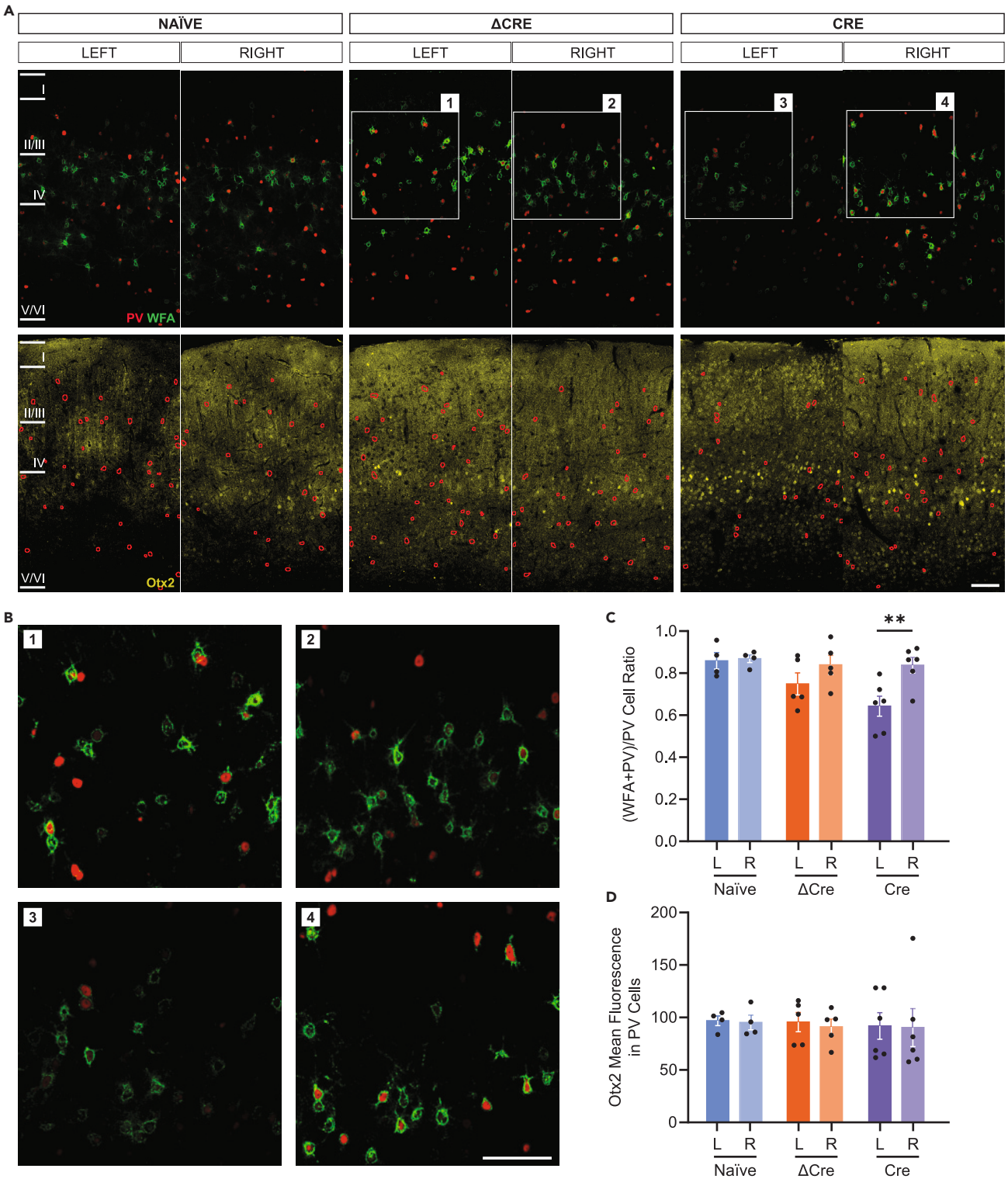

Figure 9. The amblyopia recovery after reverse suture in REST cKO is associated with a lower number of PV-positive cells surrounded by PNNs

(A) Representative confocal images of left and right Oc1b from naive (left column), ΔCre-transduced (center column) and Cre-transduced (right column) REST^{GTi} mice, immunolabelled for parvalbumin and WFA (red and green respectively, first row) and Otx2 (yellow, second row). Outlines of PV cells are superimposed onto Otx2 images to show the ROIs that were analyzed (red). The PV channel has been denoised to clearly illustrate cell somata.

Figure 9. *Continued*

(B) High magnification of layers II, III and IV from the corresponding images in panel a: ΔCre-transduced left Oc1b (1); ΔCre-transduced right Oc1b (2); Cre-transduced left Oc1b (3); Cre-transduced right Oc1b (4). Scale bars, 100 μm.

(C) Bar plot of the ratio of the number of PV neurons ensheathed by PNNs to total PV neurons, with superimposed individual experimental points. The Cre-transduced cortical area contralateral to the deprived eye shows a marked decrease in PV/PNN-positive cells with respect to the untreated contralateral hemisphere.

(D) No changes were observed in the Otx2 mean fluorescence of PV neurons. Bar plots show means ± s.e.m. with superimposed individual experimental data. **p < 00.1 one-way ANOVA/Dunnett's tests (n = 4, 5 and 6 for naive, ΔCre- and Cre-transduced mice, respectively). For exact p values and source data, see Data S1. See also Figures S3 and S6.

Italy) for assistance in breeding the mice; drs. Diego Moruzzo and Arta Mehilli (Istituto Italiano di Tecnologia, Genova, Italy) for help in genotyping; drs. Ilaria Dallorto and Rossana Ciancio (Istituto Italiano di Tecnologia, Genova, Italy) for administrative assistance. The study was supported by research grants from the Italian Ministry of University and Research (PRIN 2020-WMSNBL and PRIN 2022-XWEYBN to FB and JFMV), Compagnia di San Paolo Torino (ID ROL34760 to FB), Tuscany Health Ecosystem - THE - European Union Next-Generation EU - National Recovery and Resilience Plan (NRRP) - Mission 4 Component 2, Investment N.1.5 - CUP N. I53C22000780001 (to JFMV), IRCCS Ospedale Policlinico San Martino (Ricerca Corrente and "5x1000" to FB).

AUTHOR CONTRIBUTIONS

D.S. carried out the surgical procedures, *in vivo* electrophysiological experiments and immunohistochemical analyses; G.M. ran the molecular biology and behavioral experiments; T.F. generated the REST^{GTi} mouse; F.B. and J.F.M.V. conceived the study, analyzed the experimental data, and wrote the manuscript; F.B. financially supported the study. All authors critically discussed the experimental results and contributed to manuscript writing and revision.

DECLARATION OF INTERESTS

The authors have no relevant financial or non-financial interests to disclose.

Received: September 27, 2023
Revised: January 30, 2024
Accepted: March 13, 2024
Published: March 14, 2024

REFERENCES

1. Sale, A., Berardi, N., and Maffei, L. (2014). Environment and brain plasticity: towards and endogenous pharmacology. Physiol. Rev. *94*, 189–234.
2. Hübener, M., and Bonhoeffer, T. (2014). Neuronal plasticity: beyond the critical period. Cell *159*, 727–737.
3. Espinosa, J.S., and Stryker, M.P. (2012). Development and plasticity of the primary visual cortex. Neuron *75*, 230–249.
4. Maya-Vetencourt, J.F., Tiraboschi, E., Spolidoro, M., Castrén, E., and Maffei, L. (2011). Serotonin triggers a transient epigenetic mechanism that reinstates adult visual cortex plasticity in rats. Eur. J. Neurosci. *33*, 49–57.
5. West, A.E., Griffith, E.C., and Greenberg, M.E. (2002). Regulation of transcription factors by neuronal activity. Nat. Rev. Neurosci. *3*, 921–931.
6. Yap, E.-L., and Greenberg, M.E. (2018). Activity-regulated transcription: bridging the gap between neuronal activity and behavior. Neuron *100*, 330–348.
7. Bruce, A.W., Donaldson, I.J., Wood, I.C., Yerbury, S.A., Sadowski, M.I., Chapman, M., Göttgens, B., and Buckley, N.J. (2004). Genome-wide analysis of repressor element 1 silencing transcription factor/neuron-restrictive silencing factor (REST/NRSF) target genes. Proc. Natl. Acad. Sci. USA *101*, 10458–10463.
8. Schoenherr, C.J., and Anderson, D.J. (1995). The neuron-restrictive silencing factor (NRSF): a coordinate repressor of multiple neuron-specific genes. Science *267*, 1360–1363.
9. Grimes, J.A., Nielsen, S.J., Battaglioli, E., Miska, E.A., Speh, J.C., Berry, D.L., Atouf, F., Holdener, B.C., Mandel, G., and Kouzarides, T. (2000). The co-repressor mSin3A is a functional component of the REST-CoREST repressor complex. J. Biol. Chem. *275*, 9461–9467.
10. Abrajano, J.J., Qureshi, I.A., Gokhan, S., Zheng, D., Bergman, A., and Mehler, M.F. (2009). REST and CoREST modulate neuronal subtype specification, maturation and maintenance. PLoS One *4*, 7936.
11. Andrés, M.E., Burger, C., Peral-Rubio, M.J., Battaglioli, E., Anderson, M.E., Grimes, J., Dallman, J., Ballas, N., and Mandel, G. (1999). CoREST: a functional corepressor required for regulation of neural-specific gene expression. Proc. Natl. Acad. Sci. USA *96*, 9873–9878.
12. Ballas, N., and Mandel, G. (2005). The many faces of REST oversee epigenetic programming of neuronal genes. Curr. Opin. Neurobiol. *15*, 500–506.
13. Ooi, L., and Wood, I.C. (2007). Chromatin crosstalk in development and disease: lessons from REST. Nat. Rev. Genet. *8*, 544–554.
14. Chen, Z.F., Paquette, A.J., and Anderson, D.J. (1998). NRSF/REST is required in vivo for repression of multiple neuronal target genes during embryogenesis. Nat. Genet. *20*, 136–142.
15. Ballas, N., Grunseich, C., Lu, D.D., Speh, J.C., and Mandel, G. (2005). REST and its corepressors mediate plasticity of neuronal gene chromatin throughout neurogenesis. Cell *121*, 645–657.
16. Pozzi, D., Lignani, G., Ferrea, E., Contestabile, A., Paonessa, F., D'Alessandro, R., Lippiello, P., Boido, D., Fassio, A., Meldolesi, J., et al. (2013). REST/NRSF-mediated intrinsic homeostasis protects neuronal networks from hyperexcitability. EMBO J. *32*, 2994–3007.
17. Pecoraro-Bisogni, F., Lignani, G., Contestabile, A., Castroflorio, E., Pozzi, D., Rocchi, A., Prestigio, C., Orlando, M., Valente, P., Massacesi, M., et al. (2018). REST-dependent presynaptic homeostasis induced by chronic neuronal hyperactivity. Mol. Neurobiol. *55*, 4959–4972.
18. Prestigio, C., Ferrante, D., Marte, A., Romei, A., Lignani, G., Onofri, F., Valente, P., Benfenati, F., and Baldelli, P. (2021). REST/NRSF drives homeostatic plasticity of inhibitory synapses in a target-dependent fashion. Elife *10*, 69058.
19. Hu, X.-L., Cheng, X., Cai, L., Tan, G.-H., Xu, L., Feng, X.Y., Lu, T.J., Xiong, H., Fei, J., and Xiong, Z.Q. (2011). Conditional deletion of

NRSF in forebrain neurons accelerates epileptogenesis in the kindling model. Cerebr. Cortex *21*, 2158–2165.
20. Palm, K., Belluardo, N., Metsis, M., and Timmusk, T. (1998). Neuronal expression of zinc finger transcription factor REST/NRSF/XBR gene. J. Neurosci. *18*, 1280–1296.
21. Spencer, E.M., Chandler, K.E., Haddley, K., Howard, M.R., Hughes, D., Belyaev, N.D., Coulson, J.M., Stewart, J.P., Buckley, N.J., Kipar, A., et al. (2006). Regulation and role of REST and REST4 variants in modulation of gene expression in vivo and in vitro in epilepsy models. Neurobiol. Dis. *24*, 41–52.
22. Lu, T., Aron, L., Zullo, J., Pan, Y., Kim, H., Chen, Y., Yang, T.H., Kim, H.M., Colaiácovo, M.P., Liu, X.S., et al. (2014). REST and stress resistance in ageing and Alzheimer's disease. Nature *507*, 448–454.
23. Zullo, J.M., Drake, D., Aron, L., O'Hern, P., Dhamne, S.C., Davidsohn, N., Mao, C.A., Klein, W.H., Rotenberg, A., Bennett, D.A., et al. (2019). Regulation of lifespan by neural excitation and REST. Nature *574*, 359–364.
24. Mrsic-Flogel, T.D., Hofer, S.B., Ohki, K., Reid, R.C., Bonhoeffer, T., and Hübener, M. (2007). Homeostatic regulation of eye-specific responses in visual cortex during ocular dominance plasticity. Neuron *54*, 961–972.
25. Maya-Vetencourt, J.F., and Origlia, N. (2012). Visual cortex plasticity: a complex interplay of genetic and environmental influences. Neural Plast. *2012*, 631965.
26. Maya-Vetencourt, J.F., and Pizzorusso, T. (2013). Molecular mechanisms at the basis of plasticity in the developing visual cortex: epigenetic processes and gene programs. J. Exp. Neurosci. *7*, 75–83.
27. Putignano, E., Lonetti, G., Cancedda, L., Ratto, G., Costa, M., Maffei, L., and Pizzorusso, T. (2007). Developmental downregulation of histone posttranslational modifications regulates visual cortical plasticity. Neuron *53*, 747–759.
28. Fagiolini, M., and Hensch, T.K. (2000). Inhibitory threshold for critical-period activation in primary visual cortex. Nature *404*, 183–186.
29. Hensch, T. (2005). Critical period plasticity in local cortical circuits. Nat. Rev. Neurosci. *6*, 877–888.
30. Sugiyama, S., Di Nardo, A.A., Aizawa, S., Matsuo, I., Volovitch, M., Prochiantz, A., and Hensch, T.K. (2008). Experience-dependent transfer of Otx2 homeoprotein into the visual cortex activates postnatal plasticity. Cell *134*, 508–520.
31. Berardi, N., Pizzorusso, T., and Maffei, L. (2004). Extracellular matrix and visual cortical plasticity: freeing the synapse. Neuron *44*, 905–908.
32. Bernard, C., and Prochiantz, A. (2016). Otx2-PNN interaction to regulate cortical plasticity. Neural Plast. *2016*, 7931693.
33. Faini, G., Aguirre, A., Landi, S., Lamers, D., Pizzorusso, T., Ratto, G.M., Deleuze, C., and Bacci, A. (2018). Perineuronal nets control visual input via thalamic recruitment of cortical PV interneurons. Elife *7*, 41520.
34. Ribot, J., Breton, R., Calvo, C.F., Moulard, J., Ezan, P., Zapata, J., Samama, K., Moreau, M., Bemelmans, A.P., Sabatet, V., et al. (2021). Astrocytes close the mouse critical period for visual plasticity. Science *373*, 77–81.
35. Essenfelder, G.M., Larderet, G., Waksman, G., and Lamartine, J. (2005). Gene structure and promoter analysis of the human GJB6 gene encoding connexin 30. Gene *350*, 33–40.
36. Oyamada, M., Takebe, K., and Oyamada, Y. (2013). Regulation of connexin expression by transcription factors and epigenetic mechanisms. Biochim. Biophys. Acta *1828*, 118–133.
37. Gordon, J.A., and Stryker, M.P. (1996). Experience-dependent plasticity of binocular responses in the primary visual cortex of the mouse. J. Neurosci. *16*, 3274–3286.
38. Frenkel, M.Y., and Bear, M.F. (2004). How monocular deprivation shifts ocular dominance in visual cortex of young mice. Neuron *44*, 917–923.
39. Sawtell, N.B., Frenkel, M.Y., Philpot, B.D., Nakazawa, K., Tonegawa, S., and Bear, M.F. (2003). NMDA receptor-dependent ocular dominance plasticity in adult visual cortex. Neuron *38*, 977–985.
40. Beurdeley, M., Spatazza, J., Lee, H.H.C., Sugiyama, S., Bernard, C., Di Nardo, A.A., Hensch, T.K., and Prochiantz, A. (2012). Otx2 binding to perineuronal nets persistently regulates plasticity in the mature visual cortex. J. Neurosci. *32*, 9429–9437.
41. Watakabe, A., Ohtsuka, M., Kinoshita, M., Takaji, M., Isa, K., Mizukami, H., Ozawa, K., Isa, T., and Yamamori, T. (2015). Comparative analyses of adeno-associated viral vector serotypes 1, 2, 5, 8 and 9 in marmoset, mouse and macaque cerebral cortex. Neurosci. Res. *93*, 144–157.
42. Pizzorusso, T., Medini, P., Berardi, N., Chierzi, S., Fawcett, J.W., and Maffei, L. (2002). Reactivation of ocular dominance plasticity in the adult visual cortex. Science *298*, 1248–1251.
43. He, H.Y., Hodos, W., and Quinlan, E.M. (2006). Visual deprivation reactivates ocular dominance plasticity in adult visual cortex. J. Neurosci. *26*, 2951–2955.
44. Maya-Vetencourt, J.F., Sale, A., Viegi, A., Baroncelli, L., De Pasquale, R., O'Leary, O.F., Castrén, E., and Maffei, L. (2008). The antidepressant fluoxetine restores plasticity in the adult visual cortex. Science *320*, 385–388.
45. Maya-Vetencourt, J.F., Tiraboschi, E., Greco, D., Restani, L., Cerri, C., Auvinen, P., Maffei, L., and Castrén, E. (2012). Experience-dependent expression of Npas4 regulates plasticity in adult visual cortex. J. Physiol. *590*, 4777–4787.
46. Baroncelli, L., Sale, A., Viegi, A., Maya Vetencourt, J.F., De Pasquale, R., Baldini, S., and Maffei, L. (2010). Experience-dependent reactivation of ocular dominance plasticity in the adult visual cortex. Exp. Neurol. *226*, 100–109.
47. Tiraboschi, E., Guirado, R., Greco, D., Auvinen, P., Maya-Vetencourt, J.F., Maffei, L., and Castrén, E. (2013). Gene expression patterns underlying the reinstatement of plasticity in the adult visual system. Neural Plast. *2013*, 605079.
48. Harauzov, A., Spolidoro, M., DiCristo, G., De Pasquale, R., Cancedda, L., Pizzorusso, T., Viegi, A., Berardi, N., and Maffei, L. (2010). Reducing intracortical inhibition in the adult visual cortex promotes ocular dominance plasticity. J. Neurosci. *30*, 361–371.
49. Morishita, H., Miwa, J.M., Heintz, N., and Hensch, T.K. (2010). Lynx1, a cholinergic brake, limits plasticity in adult visual cortex. Science *330*, 1238–1240.
50. Silingardi, D., Scali, M., Belluomini, G., and Pizzorusso, T. (2010). Epigenetic treatments of adult rats promote recovery from visual acuity deficits induced by long-term monocular deprivation. Eur. J. Neurosci. *31*, 2185–2192.
51. Cerri, C., Fabbri, A., Vannini, E., Spolidoro, M., Costa, M., Maffei, L., Fiorentini, C., and Caleo, M. (2011). Activation of Rho GTPases triggers structural remodeling and functional plasticity in the adult rat visual cortex. J. Neurosci. *31*, 15163–15172.
52. Lupori, L., Cornuti, S., Mazziotti, R., Borghi, E., Ottaviano, E., Cas, M.D., Sagona, G., Pizzorusso, T., and Tognini, P. (2022). The gut microbiota of environmentally enriched mice regulates visual cortical plasticity. Cell Rep. *38*, 110212.
53. Napoli, D., Lupori, L., Mazziotti, R., Sagona, G., Bagnoli, S., Samad, M., Sacramento, E.K., Kirkpartick, J., Putignano, E., Chen, S., et al. (2020). MiR-29 coordinates age-dependent plasticity brakes in the adult visual cortex. EMBO Rep. *21*. https://doi.org/10.15252/embr.202050431.
54. Maya-Vetencourt, J.F., Sale, A., Viegi, A., Baroncelli, L., De Pasquale, R., O'Leary, O.F., Castrén, E., and Maffei, L. (2008). The antidepressant fluoxetine restores plasticity in the adult visual cortex. Science *320*, 385–388. https://doi.org/10.1126/science.1150516.
55. Lehmann, K., and Löwel, S. (2008). Age-dependent ocular dominance plasticity in adult mice. PLoS One *3*, 3120.
56. Centonze, E., Marte, A., Albini, M., Rocchi, A., Cesca, F., Chiacchiaretta, M., Floss, T., Baldelli, P., Ferroni, S., Benfenati, F., and Valente, P. (2023). Neuron-restrictive silencer factor/repressor element 1-silencing transcription factor (NRSF/REST) controls spatial K+ buffering in primary cortical astrocytes. J. Neurochem. *165*, 701–721.
57. Winkel, F., Ryazantseva, M., Voigt, M.B., Didio, G., Lilja, A., Llach Pou, M., Steinzeig, A., Harkki, J., Englund, J., Khirug, S., et al. (2021). Pharmacological and optical activation of TrkB in Parvalbumin interneurons regulate intrinsic states to orchestrate cortical plasticity. Mol. Psychiatr. *26*, 7247–7256.
58. Shen, Y., Tenney, A.P., Busch, S.A., Horn, K.P., Cuascut, F.X., Liu, K., He, Z., Silver, J., and Flanagan, J.G. (2009). PTPsigma is a receptor for chondroitin sulfate proteoglycan, an inhibitor of neural regeneration. Science *326*, 592–596.
59. Lesnikova, A., Casarotto, P.C., Fred, S.M., Voipio, M., Winkel, F., Steinzeig, A., Antila, H., Umemori, J., Biojone, C., and Castrén, E. (2021). Chondroitinase and antidepressants promote plasticity by releasing TrkB from dephosphorylating control of PTPsigma in parvalbumin neurons. J. Neurosci. *41*, 972–980.
60. Lin, Y., Bloodgood, B.L., Hauser, J.L., Lapan, A.D., Koon, A.C., Kim, T.K., Hu, L.S., Malik, A.N., and Greenberg, M.E. (2008). Activity-dependent regulation of inhibitory synapse development by Npas4. Nature *455*, 1198–1204.
61. Bloodgood, B.L., Sharma, N., Browne, H.A., Trepman, A.Z., and Greenberg, M.E. (2013). The activity-dependent transcription factor NPAS4 regulates domain-specific inhibition. Nature *503*, 121–125.
62. Ramamoorthi, K., Fropf, R., Belfort, G.M., Fitzmaurice, H.L., McKinney, R.M., Neve, R.L., Otto, T., and Lin, Y. (2011). Npas4 regulates a transcriptional program in CA3 required for contextual memory formation. Science *334*, 1669–1675.

63. Sun, X., Bernstein, M.J., Meng, M., Rao, S., Sørensen, A.T., Yao, L., Zhang, X., Anikeeva, P.O., and Lin, Y. (2020). Functionally distinct neuronal ensembles within the memory engram. Cell *181*, 410–423.e17.
64. Pizzorusso, T., Medini, P., Landi, S., Baldini, S., Berardi, N., and Maffei, L. (2006). Structural and functional recovery from early monocular deprivation in adult rats. Proc. Natl. Acad. Sci. USA *103*, 8517–8522.
65. Cannarozzo, C., Rubiolo, A., Casarotto, P., and Castrén, E. (2023). Ketamine and its metabolite 2R,6R-hydroxynorketamine promote ocular dominance plasticity and release tropomyosin-related kinase B from inhibitory control without reducing perineuronal nets enwrapping parvalbumin interneurons. Eur. J. Neurosci. *57*, 940–950.
66. Sale, A., Maya-Vetencourt, J.F., Medini, P., Cenni, M.C., Baroncelli, L., De Pasquale, R., and Maffei, L. (2007). Environmental enrichment in adulthood promotes amblyopia recovery through a reduction of intracortical inhibition. Nat. Neurosci. *10*, 679–681.
67. Lunghi, C., Sframeli, A.T., Lepri, A., Lepri, M., Lisi, D., Sale, A., and Morrone, M.C. (2019). A new counterintuitive training for adult amblyopia. Ann. Clin. Transl. Neurol. *6*, 274–284.
68. Polat, U., Ma-Naim, T., Belkin, M., and Sagi, D. (2004). Improving vision in adult amblyopia by perceptual learning. Proc. Natl. Acad. Sci. USA *101*, 6692–6697.
69. Huang, C.B., Zhou, Y., and Lu, Z.L. (2008). Broad bandwidth of perceptual learning in the visual system of adults with anisometropic amblyopia. Proc. Natl. Acad. Sci. USA *105*, 4068–4073.
70. Li, R.W., Ngo, C., Nguyen, J., and Levi, D.M. (2011). Video-game play induces plasticity in the visual system of adults with amblyopia. PLoS One *9*, 1001135.
71. Wu, C., Gaier, E.D., Nihalani, B.R., Whitecross, S., Hensch, T.K., and Hunter, D.G. (2023). Durable recovery from amblyopia with donepezil. Sci. Rep. *13*, 10161.
72. Kaeser, P.S., Deng, L., Wang, Y., Dulubova, I., Liu, X., Rizo, J., and Südhof, T.C. (2011). RIM Proteins Tether Ca2+ Channels to Presynaptic Active Zones via a Direct PDZ-Domain Interaction. Cell *144*, 282–295.
73. Nechiporuk, T., McGann, J., Mullendorff, K., Hsieh, J., Wurst, W., Floss, T., and Mandel, G. (2016). The REST remodeling complex protects genomic integrity during embryonic neurogenesis. Elife *5*, 09584.
74. Kretschmer, F., Sajgo, S., Kretschmer, V., and Badea, T.C. (2015). A system to measure the optokinetic and optomotor response in mice. J. Neurosci. Methods *256*, 91–105.
75. Kretschmer, F., Kretschmer, V., Kunze, V.P., and Kretzberg, J. (2013). OMR-arena: automated measurement and stimulation system to determine mouse visual thresholds based on optomotor responses. PLoS One *8*, 78058.
76. Vandesompele, J., De Preter, K., Pattyn, F., Poppe, B., Van Roy, N., De Paepe, A., and Speleman, F. (2002). Accurate normalization of real-time quantitative RT-PCR data by geometric averaging of multiple internal control genes. Genome Biol. *3*, 0034.

STAR★METHODS

KEY RESOURCES TABLE

REAGENT or RESOURCE	SOURCE	IDENTIFIER
Antibodies		
Biotinylated *Wisteria floribunda* agglutinin	Vector Biolabs	cat#B1355; RRID: AB_2336874
Guinea pig monoclonal anti-PV antibody	Synaptic Systems	cat#195-004; RRID: AB_2156476
Rabbit polyclonal anti-Otx2 antibody	Proteintech	cat#134971-AP; RRID: AB_2157176
Streptavidin + Dylight®594	Vector Biolabs	cat#SA-5594-1; RRID: AB_2336418
Alexa Fluor® 405-conjugated goat anti-rabbit	Thermo Fisher	cat#A-31556; RRID: AB_221605
Alexa Fluor® 647-conjugated goat anti-guinea pig	Thermo Fisher	cat#A-21450; RRID: AB_2535867
Bacterial and virus strains		
AAV9-CMV-eGFP-2A-iCre	Vector Biolabs	cat#7099
AAV9-CMV-eGFP-2A-ΔCre	Vector Biolabs; Kaeser et al., 2011[72]	N/A
Experimental models: Organisms/strains		
Mouse: $REST^{GTi}$: $Rest^{GTi(D047E11)}$	Gail Mandel (Portland, United States); Nechiporuk et al., 2016[73]	N/A
Oligonucleotides		
Primers for RT-PCR, see Table S1	Sigma-Aldrich; Eurofins Genomics	N/A
Deposited data		
Source data and statistics	This paper	Supplemental File *Source Data.xlsx*
Software and algorithms		
ImageJ	NIH	https://imagej.nih.gov/ij/
Prism 10	Graphpad Software	https://www.graphpad.com/features
MATLAB	Mathworks	https://www.mathworks.com/products/matlab.html
Synapse	Tucker-Davis Technologies	https://www.tdt.com/
Other		
ZIF-Clip chronic implantable arrays	Tucker-Davis Technologies	cat#ZIF201016

RESOURCE AVAILABILITY

Lead contact

Further information and requests for resources and reagents should be directed to and will be fulfilled by the lead contact, **Prof. Fabio Benfenati** (Fabio.benfenati@iit.it).

Materials availability

This study did not generate new unique reagents.

Data and code availability

- Source data for all figures is included in the supplementary Source Data and Statistics file.
- This paper does not report original code.
- Any additional information required to reanalyze the data reported in this paper is available from the lead contact upon request.

EXPERIMENTAL MODEL AND STUDY PARTICIPANT DETAILS

Murine model

Heterozygous GTinv-REST mice ($REST^{GTi}$ mice[73]) were kindly provided by Gail Mandel (Portland, United States) and the German Gene Trap Consortium (GGTC-Partners). The $REST^{GTi}$ mouse strain has an inverted GTinv cassette between exons 1 and 2 of the Rest gene. Inducing

expression of Cre recombinase re-inverts the cassette (GTre-inv) and results in a mutant REST allele in which exons 1a–1c are spliced to the β-geo gene instead of exon 2. This truncates transcription, and expression of REST.[73] Animals of both sexes were maintained in a C57BL/6J background and kept in homozygosity. Mice were housed on a 12:12 h light/dark cycle (lights on at 7 a.m.) at constant temperature (22 ± 1°C) and relative humidity (60 ± 10%), provided drinking water and a complete pellet diet (Mucedola, Settimo Milanese, Italy) *ad libitum* under conditions of environmental enrichment in the IRCCS Ospedale Policlinico San Martino Animal Facility. All efforts were made to minimize suffering and reduce the number of animals used. All experiments were carried out in accordance with the guidelines established by the European Community Council (Directive 2010/63/EU of 22 September 2010) and were approved by the Italian Ministry of Health (Authorization #427/2021-PR).

Animals of both sexes were used, and precise ages at the time of experimental procedures are detailed in the manuscript.

METHOD DETAILS

Intracortical microinjection for AAV-mediated transduction

The AAV9 preparations used for inducing were: (i) Cre recombinase (AAV9-CMV-eGFP-2A-iCre, Vector Biolabs cat#7099) and (ii) recombinase dead ΔCre (AAV9-CMV-eGFP-2A-ΔCre; custom ordered from Vector Biolabs per Kaeser et al., 2011[72]), with recombinase and eGFP reported expressed by the same CMV promoter together with the self-cleaving 2A peptide. $REST^{GTi}$ mice were first anesthetized with 2% isoflurane in an induction chamber, and then transferred to a stereotaxic frame inside a sterile microsurgery hood, where their head was fixed with ear bars and the muzzle comfortably secured into the nosecone. Isoflurane was then gradually lowered to around 1.8% and paw, tail and ear pinch reflexes were tested to verify adequate anesthesia before proceeding. A drop of sterile 0.9% saline solution was applied to each eye to maintain hydration. The scalp was dabbed and scrubbed with iodopovidone (Betadine). The scalp above the left occiput was cut with surgical scissors to expose the underlying skull, and the epicranial aponeurosis and pericranium were delicately scraped off. A fine tip marker was secured into the stereotaxic arm, centered on the lambda suture, and used to mark the coordinates of 4 injection points on the skull, corresponding to the mouse Oc1b ([-2L;0AP],[-2.9L;0AP],[-2L;0.5AP],[-2.9L;0.5AP], all in mm). Holes were then drilled at the marks. A Hamilton Gastight syringe with a flat-tip needle was then mounted into the stereotaxic arm and 800 nL of the AAV solution was drawn in using a Stoelting QSI microinjection pump. The stereotaxic apparatus was then used to guide the needle into each injection site at 100 μm depth. The AAV9 suspension (200 nL; titer: $1x10^{13}$ GC/ml) was slowly (100 nl/min) infused into each site, followed by a 2-min pause to allow virus diffusion. The syringe was then withdrawn, the skull irrigated with sterile saline and scalp incision closed by an absorbable suture. Post-operative analgesia was administered via intramuscular hindlimb injection of diclofenac.

Chronic microwire array implants

Preparatory steps to first incision were executed as per injection. Three weeks after transduction, a sagittal incision from bregma to lambda was performed and ca. 1-1.5 mm of scalp was trimmed from each flap edge. Debridement, scraping and irrigation of the underlying tissue was performed as necessary to clearly expose the cranial surface. A thin layer of 35% H_3PO_4 solution in ddH_2O was then applied to the bone for ca. 20 s to slightly demineralize the surface and prime it for cement adhesion. Abundant irrigation with saline and wiping off was repeated to remove the acid. Holes were then drilled in the left side of the frontal bone and posterior right parietal bone to accommodate ground and reference microscrews. Previous injection hole scars were identified, and an area of bone large enough to fit the implant array was milled out with the bone drill. After irrigation and cleanup, the exposed dura mater was removed with fine-tip forceps. We used 16-channel implants (ZIF2010-16 array, Tucker-Davis Technologies) with 2 rows of 8 wires, each having a diameter of 50 μm and spaced 250 μm from each other. The space between the two rows is 375 μm. Each microwire has a tip taper angle of 60° for less traumatic implantation. The implant was mounted onto a holder clip in the stereotaxic arm and inserted into the Oc1b at a depth of 400 μm. The bone opening around the array was then sealed with Quik-Sil tissue sealant (World Precision Instruments) and allowed to set. The array's ground and reference wires were then wound around the corresponding screws, and the excess was trimmed. Antibiotic-loaded PMMA dental cement (7 mg gentamicin powder, Sigma, per 1 g cement powder, Paladur) was applied to fix the implant, cover the area, and provide long-term infection prophylaxis. Once set, the stereotaxic mount was unclipped and removed, and a protective cap was applied to the implant connectors and secured with tape. Post-operative analgesia was administered via intramuscular hindlimb injection of diclofenac.

In vivo electrophysiology

Electrophysiology in freely moving awake mice

After 3 days of MD, freely moving, awake visual evoked potential recordings in a 60x60x60cm transparent enclosure were performed using a Tucker-Davis Technologies recording setup. This consists of a recording computer running Synapse software interfaced with a TDT RZ5D signal processor/amplifier unit, receiving input from the rotary joint and implant headstage through a PZ5 pre-amp. The visual stimulus was provided by a white LED (Thorlabs MNWHL4, 186lx/67cd) triggered by the setup. Three single flash durations were employed in subsequent experiments: 0 (blank), 100 and 200 ms. Continuous local field potential (LFP) readouts and peri-stimulus snippets ("VEP Sweeps") were sampled at 1017 Hz and stored by the program. The LFP feed was band-pass filtered 1-100 Hz and each sweep included 200 ms of pre-stimulus time and 600 ms of post-stimulus activity. Sweep period was set to 2 s with a 42% jitter to minimize noise-related error. At least 50 sweeps were recorded per stimulus type to obtain the average for each channel. Noise was calculated averaging the 200 ms pre-stimulus period (baseline). VEPs with peak-to-baseline amplitude ≥5 standard deviations of the noise band were considered significant. Offline analysis

was performed using the TDT MATLAB SDK tools. To obtain the baseline ("*Before*") C/I ratio, the responses from each eye were recorded independently. The non-recorded eye was temporarily closed by monocular suture placed under brief anesthesia. After the intervention, the eyes were given tobramycin/dexamethasone eye drops to avoid infection. Following anesthesia recovery, the animals were then placed in the enclosure, connected to the setup and recordings executed for all stimulus durations. The eye contralateral to the transduced cortex was left deprived for 3 days, following which recordings from each eye were performed again to monitor any changes in OD. The C/I ratios obtained from the signals of the 16 channels were averaged to obtain the overall ratio.

Electrophysiology in anesthetized mice (amblyopia model)

To reduce the number of anesthesia inductions, the recordings for the amblyopic paradigm were performed under isoflurane anesthesia. The gas mixture was fed through a nosecone to the animal fixed in the center of the enclosure. All other elements of the recording setup were as previously described. Before recording, the long-term deprived eye contralateral to the treated cortex was carefully opened with surgical scissors. The responses from each eye were recorded independently ("*Before*"), by alternately closing them. The animals were connected to the setup and recordings executed for all stimulus durations. The ipsilateral eye to the treated cortex was then left deprived for 15 days, after which recordings for both eyes were performed again to monitor any changes in OD ("*After*").

Optomotor response

The optomotor response was determined using a qOMR apparatus consisting of a box whose vertical faces are internally lined with 4 screens facing a raised central platform. The lower and upper faces are internally mirrored, creating the illusion of infinite depth, with the upper lid mounting a camera. Our experimental protocol was comprised of stimuli at increasing spatial frequencies (0.012, 0.05, 0.1, 0.15, 0.2, 0.3, and 0.4 cycles per degree, c/deg), intercalated by a gray screen. Each stimulus was randomly presented for 60 s at a movement speed of 12 deg/s. The protocol was repeated 4 times ("trials") and the scores for each spatial frequency were individually averaged to produce the final readout curve showing the performance at all spatial frequencies. The analyses were normally performed along two days (2 trials per day) to avoid stressing the animals. The software also performed separation of single eye components, by analyzing clockwise and counterclockwise rotations, and attributing OMR ratios to the left and right eye, respectively.[74,75] The score of 1.0 was taken as a cut-off for sensory perception: animals with qOMR scores < 1 were considered not to perceive the spatial frequency under investigation. The OMR AUC was calculated respect to y=1 (positive area when f(x)>1; negative area when f(x)<1).

Real-time qPCR

Cre and ΔCre-transduced animals were euthanized by CO_2 inhalation followed by cervical dislocation 3-4 weeks after AAV administration. Brains were explanted and the left and right V1 dissected and harvested. Total RNA from brain tissue was isolated with Trizol (Invitrogen) according to the manufacturer's instructions, and reverse transcribed into cDNA using the SuperScript IV First-Strand Synthesis System (Invitrogen). Gene expression was measured by qRT-PCR using the CFX96 Touch Real-Time PCR Detection System (Biorad). *Gapdh* and *Actin* were used as housekeeping genes. The relative gene expression was determined using the $2^{-\Delta\Delta CT}$ method.[76] Individual data were normalized on the mean of ΔCre group. qRT-PCR primers used can be found in Table S1.

Immunohistochemistry and morphometric analysis

At the end of the experimental protocols, animals were terminally anesthetized with intraperitoneal ketamine and transcardially perfused first with phosphate-buffered saline (PBS) chilled on ice, then 4% paraformaldehyde (PFA) in PBS. Brains were extracted and post-fixed for 48hrs in PFA at 4°C. The injection/implant sites were identified and sliced in a chilled PBS bath at 50 μm on a 5100mz vibratome (Campden Instruments). Slices were placed free-floating in multi-well plates, washed 3 times for 3 min in PBS for lectins (PBlec: 0.1 mM $CaCl_2$, $MnCl_2$, $MgCl_2$ in PBS) and transferred to blocking solution (10% BSA + 1% Triton X-100 in PBlec) for 1 h. They were then moved to a primary antibody/lectin bath comprised of biotinylated Wisteria floribunda agglutinin (WFA, 1:300, Vector Labs B1355), anti-PV guinea pig antibody (1:300, Synaptic Systems 195-004) and anti-Otx2 rabbit antibody (1:100, Proteintech 134971-AP) in PBlec overnight at 4 °C. After 3 washes, slices were placed in a secondary solution of Streptavidin/Dylight®594 (1:300, Vector Labs SA-5594-1), Alexa Fluor® 647-conjugated goat anti-guinea pig secondary antibody (1:300, Thermo Scientific) and Alexa Fluor® 405-conjugated goat anti-rabbit secondary antibody (1:100, Thermo Scientific) for 2 h at room temperature. After 3 more washes, slices were mounted on slides and closed with Mowiol. Imaging was performed at 40x magnification with an oil immersion objective on a Leica SP8 laser scanning confocal microscope, capturing an 800 μm-wide mosaic of ROIs comprising all cortical layers. ImageJ (NIH) software was used for quantification, sampling 10-plane z-max projections of 3 images from 3 different slices per animal, including the untreated hemisphere of each animal as internal control. Cell counts were performed manually. To isolate PV somata ROIs for Otx2 measurements, the PV channel z-max projection was binarized and filtered for shapes > 15 μm. Then, the ImageJ Analyze Particles plugin was used to outline PV cell somata.

QUANTIFICATION AND STATISTICAL ANALYSIS

The number of mice necessary for the project was preliminarily calculated based on the experimental variability and need to reach an appropriate number of replications for a robust statistical analysis and occasional loss of animals due to anesthesia or unpredictable factors. The number of animals for the planned experiments (sample size, n) was predetermined using the G*Power software according to the following

formula: $n = Z^2 \times \sigma^2 / \Delta^2$, where: Z is the value of the distribution function f(α,β) (with α and β type-I and type-II errors, respectively; based on $\alpha = 0.05$ and $1-\beta = 0.9$), σ is the standard deviation of the groups (set between 0.2-0.3 based on similar experiments and preliminary data) and Δ the minimum percent difference that is thought to be biologically relevant (0.2 or 20%). Experiments were carried out blind to the experimenter. Males and females were both used in experimental procedures. Data are expressed either as means $\pm$ s.e.m. for number of independent animals (n) with superimposition of the individual experimental points or as box plots characterized by the following elements: center line, median (Q2); cross symbol, mean; box limits, 25^{th} (Q1)-75^{th} (Q3) percentiles; whisker length refers to min-to max values. Normal distribution was assessed using the D'Agostino–Pearson normality test. To compare two normally distributed sample groups, the unpaired or paired Student's *t*-test was used. To compare two sample groups that were not normally distributed, the Mann-Whitney's *U*-test was used. To compare more than two normally distributed sample groups, one- or two-way ANOVA followed by post-hoc multiple comparisons (Holm-Šidák's or Dunnett's test). $p < 0.05$ was considered significant. Statistical analysis was carried out using Prism v9 (GraphPad Software). Principal component analysis was performed using MATLAB's *pca* function, using the alternating least squares (ALS) algorithm.